



HAL
open science

Li₂O:Li–Mn–O Disordered Rock-Salt Nanocomposites as Cathode Prelithiation Additives for High-Energy Density Li-Ion Batteries

Maria Diaz-lopez, Philip Chater, Pierre Bordet, Melanie Freire, Christian Jordy, Oleg Lebedev, Valérie Pralong

► **To cite this version:**

Maria Diaz-lopez, Philip Chater, Pierre Bordet, Melanie Freire, Christian Jordy, et al.. Li₂O:Li–Mn–O Disordered Rock-Salt Nanocomposites as Cathode Prelithiation Additives for High-Energy Density Li-Ion Batteries. *Advanced Energy Materials*, 2020, 10 (7), pp.1902788. 10.1002/aenm.201902788 . hal-03451746

HAL Id: hal-03451746

<https://hal.science/hal-03451746>

Submitted on 1 Mar 2022

HAL is a multi-disciplinary open access archive for the deposit and dissemination of scientific research documents, whether they are published or not. The documents may come from teaching and research institutions in France or abroad, or from public or private research centers.

L'archive ouverte pluridisciplinaire **HAL**, est destinée au dépôt et à la diffusion de documents scientifiques de niveau recherche, publiés ou non, émanant des établissements d'enseignement et de recherche français ou étrangers, des laboratoires publics ou privés.



Distributed under a Creative Commons Attribution 4.0 International License

Li₂O:Li–Mn–O Disordered Rock-Salt Nanocomposites as Cathode Prelithiation Additives for High-Energy Density Li-Ion Batteries

Maria Diaz-Lopez,* Philip A. Chater, Pierre Bordet, Melanie Freire, Christian Jordy, Oleg I. Lebedev, and Valerie Pralong

The irreversible loss of lithium from the cathode material during the first cycles of rechargeable Li-ion batteries notably reduces the overall cell capacity. Here, a new family of sacrificial cathode additives based on Li₂O:Li_{2/3}Mn_{1/3}O_{5/6} composites synthesized by mechanochemical alloying is reported. These nanocomposites display record (but irreversible) capacities within the Li–Mn–O systems studied, of up to 1157 mAh g⁻¹, which represents an increase of over 300% of the originally reported capacity in Li_{2/3}Mn_{1/3}O_{5/6} disordered rock salts. Such a high irreversible capacity is achieved by the reaction between Li₂O and Li_{2/3}Mn_{1/3}O_{5/6} during the first charge, where electrochemically active Li₂O acts as a Li⁺ donor. A 13% increase of the LiFePO₄ and LiCoO₂ first charge gravimetric capacities is demonstrated by the addition of only 2 wt% of the nano-sized composite in the cathode mixture. This result shows the great potential of these newly discovered sacrificial additives to counteract initial losses of Li⁺ ions and improve battery performance.

The direct contact of anode materials and lithium metal^[3,4] is a common prelithiation strategy for improving the Coulombic efficiency of the battery, although this is not exempt from several disadvantages mostly related to the use of Li metal in battery manufacture (i.e., incompatibility with ambient environments, common solvents, binders, and thermal processing). These practical challenges, are partly overcome in Stabilized Lithium Metal Powder^[5,6] SLMP, where lithium metal is suspended in hydrocarbon solvents providing stability in dry air. Interestingly, SLMP has been used as a fully lithiated anode in batteries utilizing non-lithiated V₆O₁₃ or LiV₃O₈ cathodes.^[7] More recently, the also dry air stable Li_xSi–Li₂O core–shell nanoparticles^[8] have proven an excellent prelithiation reagent and are

potentially compatible with current industrial battery fabrication methods.


As an alternative route to the arduous prelithiation of anodes demanding more reactive lithium sources leading to unstable reaction products and low battery potentials,^[3] several prelithiation additives of cathode materials have been studied.

Sacrificial salts^[9] (e.g., azides,^[10] oxocarbons, dicarboxylic acids, or hydrazides) contain oxidizable anions that lose electrons during the first charge, forming Li⁺ donors and gaseous species (e.g., CO, CO₂, or N₂) amounting to ≈70% of the salt

A recurring issue limiting the performance of Li-ion batteries is the formation of a solid electrolyte interface (SEI) during the first battery charge. 7–20% of lithium from the cathode material is irreversibly bound at the surface of graphite anodes,^[1] and it can be as high as 30% for Si,^[2] in order to form this passivation layer, which results in a loss of capacity. Several prelithiation routes incorporating sacrificial additives into the cell have been explored to alleviate irreversible capacity losses during the first charge. On the whole, sacrificial materials act as Li⁺ donors and offset the loss of active Li⁺ ions during the SEI formation.

Dr. M. Diaz-Lopez
ISIS Facility
STFC Rutherford Appleton Laboratory
Didcot OX11 0QX, UK
E-mail: maria.diaz-lopez@stfc.ac.uk

Dr. M. Diaz-Lopez, Dr. P. A. Chater
Diamond Light Source Ltd.
Diamond House
Harwell Science and Innovation Campus
Didcot OX11 0DE, UK

 The ORCID identification number(s) for the author(s) of this article can be found under <https://doi.org/10.1002/aenm.201902788>.

© 2020 The Authors. Published by WILEY-VCH Verlag GmbH & Co. KGaA, Weinheim. This is an open access article under the terms of the Creative Commons Attribution License, which permits use, distribution and reproduction in any medium, provided the original work is properly cited.

DOI: 10.1002/aenm.201902788

Dr. P. Bordet
Institut Néel
CNRS
Grenoble Alpes Université
38000 Grenoble, France

Dr. M. Freire, Dr. C. Jordy
SAFT
111-113 Bd Alfred Daney, 33074 Bordeaux, France

Dr. M. Freire, Dr. O. I. Lebedev, Dr. V. Pralong
Crismat
CNRS
Unicaen
Ensicaen
Normandie Université
14000 Caen, France

weight. In spite of the promising improved potential ranges 3–4.5 V versus Li^+/Li , the uncontrolled evolution of gases could potentially damage the battery.

Several compounds with high initial charge capacity, where nonreversible applications may be found (e.g., $\text{Li}_2\text{Mn}_2\text{O}_4$,^[11] Li_2NiO_2 ,^[12] Li_6CoO_4 ,^[13] and Li_2CuO_2 ^[14]), have shown promising results as sacrificial additives and although they offer effective compensation of Li^+ loss during the first cycle, these materials show low specific capacities of $<300 \text{ mAh g}^{-1}$.

Reversible electrochemical conversion reactions between lithium and transition metal oxides have awoken interest as both positive and negative electrodes in Li-ion batteries,^[15,16] and recently, $\text{Li}_2\text{O}:\text{M}$,^[17] $\text{Li}_2\text{S}:\text{M}$,^[18] and $\text{LiF}:\text{M}$ ^[19] nanocomposites have been presented as attractive cathode prelithiation additives, able to store more than 4 times the theoretical specific capacity of existing cathodes $\approx 500\text{--}930 \text{ mAh g}^{-1}$. The best performance is given by $\text{Li}_2\text{O}:\text{M}$ (e.g., 724, 799, and 935 mAh g^{-1} for $\text{M} = \text{Co}$, Fe , and Mn , respectively), increasing the overall capacity of a LiFePO_4 (LFP) cathode with the $\text{Li}_2\text{O}:\text{Co}$ additive by 11%.^[17] Such high capacity of sacrificial cathodes have only been improved in Li_3N reaching 1399 mAh g^{-1} during the initial charge to 4.2 V.^[20] However, Li_3N is highly reactive and incompatible with most widely used solvents in lithium-ion batteries' manufacture.

Recently, we reported the outstanding charge capacity of 350 mAh g^{-1} in nanostructured $\text{Li}_4\text{Mn}_2\text{O}_5$ ^[21] cathode material with a strongly disordered and nonstoichiometric MnO-type rock-salt (RS) structure, where 2/3 of Mn are substituted by Li and accommodating 1/6 oxygen vacancies. Thus, the chemical formula of $\text{Li}_4\text{Mn}_2\text{O}_5$ is henceforth given as $\text{Li}_{2/3}\text{Mn}_{1/3}\text{O}_{5/6}$. $\text{Li}_{2/3}\text{Mn}_{1/3}\text{O}_{5/6}$ is part of an emerging family of Li-rich cathode materials based on disordered RS structures, displaying higher capacities

(200–350 mAh g^{-1}) than Li-rich layered oxides (150–250 mAh g^{-1}). Besides their superior capacities, disordered RS offers a versatile chemical playground and several disordered RS compositions have been reported over the last few years that can present multivalent transition metals, mixed O^{2-}/F^- anions, or oxygen redox.^[22–27]

Detailed compositional, structural, and electrochemical characterizations showed that the presence of 7 mol% excess of Li_2O in the $0.07\text{Li}_2\text{O}:\text{Li}_{2/3}\text{Mn}_{1/3}\text{O}_{5/6}$ composite^[28] (previously reported as single phase $\text{Li}_4\text{Mn}_2\text{O}_5$) increased the capacity of the composite mixture by 100 mAh g^{-1} , while the capacity of single phase $\text{Li}_{2/3}\text{Mn}_{1/3}\text{O}_{5/6}$ was reduced to 250 mAh g^{-1} . In this work, we demonstrate that outstanding first charge capacities ($>1150 \text{ mAh g}^{-1}$) can be achieved by the increase of the Li_2O content in the $\text{Li}_2\text{O}:\text{Li}_{2/3}\text{Mn}_{1/3}\text{O}_{5/6}$ composite, thanks to the electrochemical activation of Li_2O acting as a Li^+ donor to the RS.

We report for the first time 35 and 55 mol% Li_2O -rich composites synthesized by mechanochemical routes^[28] with exceptional 898 and 1157 mAh g^{-1} first charge capacities (see **Figure 1**). The large capacities obtained correspond to the extraction of 1.55 and 3.04 Li^+ per $\text{Li}_{2/3}\text{Mn}_{1/3}\text{O}_{5/6}$ formula unit in 35 and 55 mol% Li_2O composites, amounting to larger quantities than originally present in the RS active material. This observation evidences an in situ reaction between Li_2O and $\text{Li}_{2/3}\text{Mn}_{1/3}\text{O}_{5/6}$ during the course of the first charge where up to 84% and 97% of lithium in Li_2O has reacted from 35 and 55 mol% Li_2O composites, respectively. Electrochemically activated Li_2O could act as a Li^+ donor and explain the continuous evolution of the first charge capacity versus Li_2O content in Figure 1f. While the addition of Li_2O can increase by 300% the theoretical capacity of $\text{Li}_{2/3}\text{Mn}_{1/3}\text{O}_{5/6}$ in the highest 55 mol% Li_2O composite, the increased capacity is only limited to the first charge;

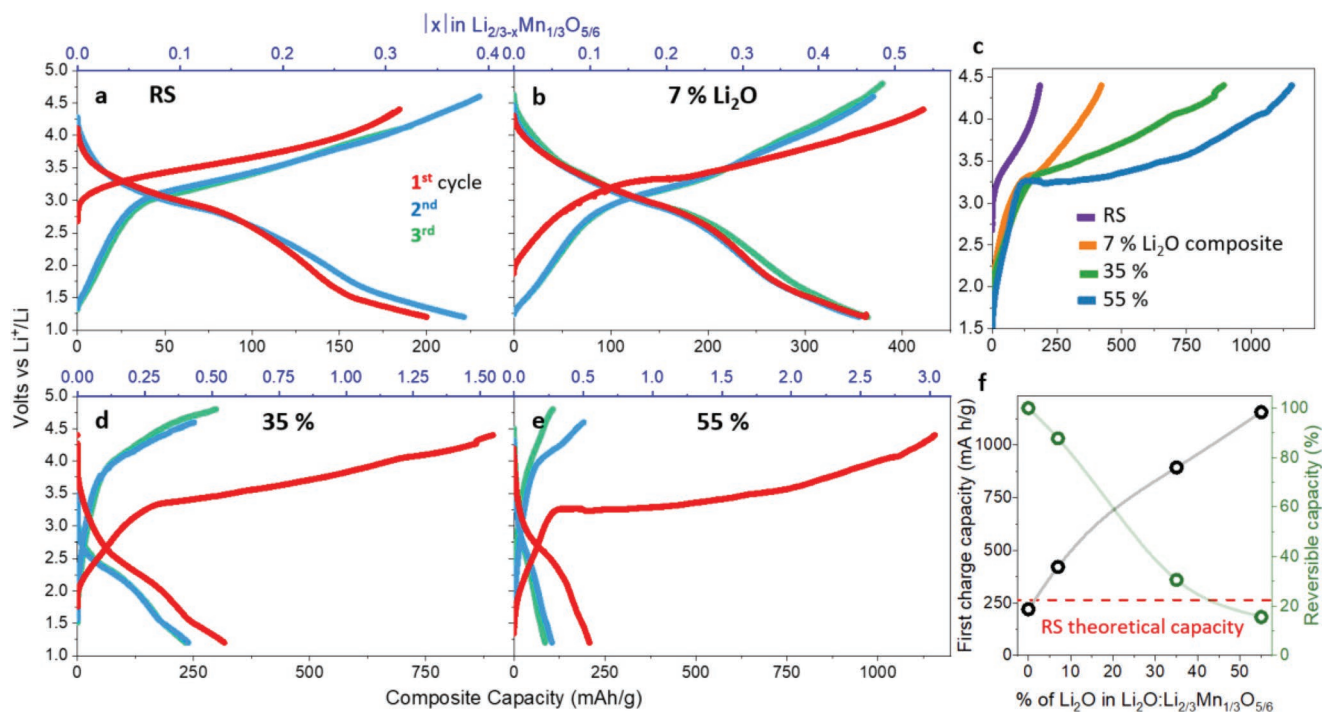


Figure 1. Voltage composition profiles of a) $\text{Li}_{2/3-x}\text{Mn}_{1/3}\text{O}_{5/6}$ RS and b,d,e) $\text{Li}_2\text{O}:\text{Li}_{2/3-x}\text{Mn}_{1/3}\text{O}_{5/6}$ composites. c) Summary of the first charge capacities for the RS and three composites studied. f) Maximum and reversible capacity versus Li_2O concentration, where the theoretical capacity of $\text{Li}_{2/3-x}\text{Mn}_{1/3}\text{O}_{5/6}$ is provided as a reference. Note that the gravimetric capacity values are expressed as a function of the total mass of composite.

and only the capacity of the active RS component is retained over the following cycles. Further increasing the Li₂O proportion did not improve the capacity further in 0.75Li₂O:0.25Li_{2/3}Mn_{1/3}O_{5/6} which displayed 914 mAh g⁻¹ first charge capacity (see Figure S1 in the Supporting Information), where only 55% of Li₂O reacted during the first charge. Although no intermediate compositions between 55% and 75% of Li₂O were studied in this work, an optimal capacity value could be found within this compositional range. The miscibility of Li₂O and Li_{2/3-x}Mn_{1/3}O_{5/6} phases at the nanoscale was demonstrated by high-resolution transmission electron microscopy images of the 0.55Li₂O:0.45Li_{2/3-x}Mn_{1/3}O_{5/6} and carbon black (30 wt%) composite in Figure S2 (Supporting Information), which shows an agglomeration of ball-shaped nanoparticles, with no clear cleavage planes, and no obvious surface layers of different compositions.

The reaction mechanisms between Li₂O and Li_{2/3}Mn_{1/3}O_{5/6} were studied by in situ total scattering. 7% and 35% Li₂O composites were studied over the course of one and two charge/discharge cycles in **Figure 2** while for the 55 mol% Li₂O-richest composite, only 20% of the first charge was recorded (see Figures S3 and S4 in the Supporting Information for in situ total scattering and ex situ diffraction and X-ray absorption near-edge spectroscopy (XANES) data for the pristine and charged at 4.5 V samples).

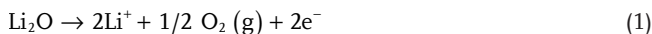
Figure 2 shows a solid solution behavior of the RS with a continuous evolution of the lattice parameters over the 1.5–4.5 V potential window, in agreement with previous in situ XANES^[29] and ex situ total scattering^[28] studies. The lattice parameter evolution, quantified by the sequential Rietveld refinement of over 100 in situ data sets, mimics the shape of the electrochemical curve. A steeper change in the lattice parameter occurs at lower potential values 2–3.5 V, following by a more gradual increase in the range 3.5–4.5 V (see Figures S6–S8 in the Supporting Information for the evolution of all sequentially refined parameters).

The nonlinear evolution of Mn–Mn interatomic distances with Li concentration in 0.07Li₂O:0.93Li_{2/3}Mn_{1/3}O_{5/6} previously characterized by extended X-ray absorption fine structure,^[29] is in good agreement with the refined lattice parameters in Figure 2a. The unit cell of the active RS phase contracts from 4.158(2) to 4.070(2) Å with the extraction of lithium after the first charge at 4.5 V, and expands to 4.126(1) Å during cell discharge. The irreversible contraction of the Li_{2/3}Mn_{1/3}O_{5/6} cell volume could be ascribed to a densification of the nanostructured RS motivated by the migration of Mn cations into cation vacancies created after the extraction of lithium. Such a material's densification would in turn explain the irreversible exchange of lithium after the first charge (≈0.15 less Li is reincorporated in the 7 mol% Li₂O composite) as a result of a lower number of cation vacancies available for lithium to migrate into. Due to the relatively low scattering power of the Li₂O component by X-rays compared to Li_{2/3}Mn_{1/3}O_{5/6}, this minority phase could not be accurately refined in the 7 mol% Li₂O composite. It was however included in the refinement of the 0.35Li₂O:0.65Li_{2/3}Mn_{1/3}O_{5/6} in situ data in Figure 2b. Note that in spite of the greater concentration of Li₂O in this nanocomposite, the Li_{2/3}Mn_{1/3}O_{5/6} component behaves in an analogous way as in 7% Li₂O, albeit a more pronounced contraction of the lattice parameters occurs during the first charge down to 4.035(3) Å. The main Bragg reflections from Li₂O in the diffraction pattern of 0.35Li₂O:0.65Li_{2/3}Mn_{1/3}O_{5/6}, highlighted with an asterisk in

Figure 2b, disappear gradually until they are no longer observed after the first charge (see Figure S7 in the Supporting Information for the refined phase wt%), and no traces of other crystalline or amorphous secondary phases could be detected. After the first charge, Li_{2/3-x}Mn_{1/3}O_{5/6} cycles reversibly between charged and discharged states with an exchange of ≈0.4 Li per formula unit without the further participation of Li₂O. In contrast to Li₂O:MO nanocomposites with 100% capacity retention over several cycles,^[15,30] the participation of Li₂O in Li₂O:Li_{2/3-x}Mn_{1/3}O_{5/6} is irreversible, which explains the large irreversible capacities in Figure 1f.

The local structural evolution of the RS phase remaining after the initial charge is investigated in more detail in Figure 2c, where the effects of the lattice parameter changes were removed by multiplying the *r*-scale by the ratio of the lattice parameters determined through Rietveld refinement. The narrow Mn–Mn distributions centered around the expected values for the average RS structure indicate that the Mn framework is well ordered, while the broader, asymmetric, and shifted Mn–O distributions indicate a high degree of disorder within the oxygen site (since Mn is well ordered, the broadness of these peaks could only be ascribed to disorder within the oxygen sites). Thus, Li_{2/3-x}Mn_{1/3}O_{5/6} is able to accommodate varying concentrations of lithium, thanks to the breathing of the cubic Mn framework that isotropically contracts and expands to extract and incorporate lithium, accompanied by displacements of oxygen atoms. It is worth noting that the evolution of the RS phase is identical to all composites, whichever the initial concentration of Li₂O.

Galvanostatic tests of mechanically milled Li₂O powders without Li_{2/3-x}Mn_{1/3}O_{5/6} failed to electrochemically decompose Li₂O. Thus, although the mechanism by which Li₂O becomes electrochemically active is not yet understood, the nanostructured Li_{2/3-x}Mn_{1/3}O_{5/6} component is expected to play a key role in catalyzing this reaction. The RS phase could catalyze the irreversible decomposition of Li₂O into Li⁺ (consumed in the cell to form the SEI) as well as O₂ (g) or superoxide radicals (O₂⁻) following the reactions.



During the experiments in Figure 2 and Figure S3 (Supporting Information) performed in transparent cells made of quartz glass, no significant bubbling of electrolyte was observed that could result from an uncontrolled evolution of O₂ (g). Thus, if O₂ release occurs, it must be formed at a slow rate through the course of the first charge over a wide potential window lapsing several hours.

As for O₂⁻, the formation of these more reactive radicals is frequently associated to decomposition reactions with the carbonate solvent,^[31] leading to the formation of CO₂, H₂O, and crystalline Li₂CO₃ or Li₂O₂ decomposition products (among other phases). However, neither crystalline nor amorphous secondary phases were detected by total scattering (see Figure S9 in the Supporting Information). Given that non-negligible amounts of Li₂CO₃ or Li₂O₂ are expected to form when all Li₂O reacts via this route in the 35 and 55 mol% Li₂O-rich composite and these are not observed, the sole decomposition into O₂⁻

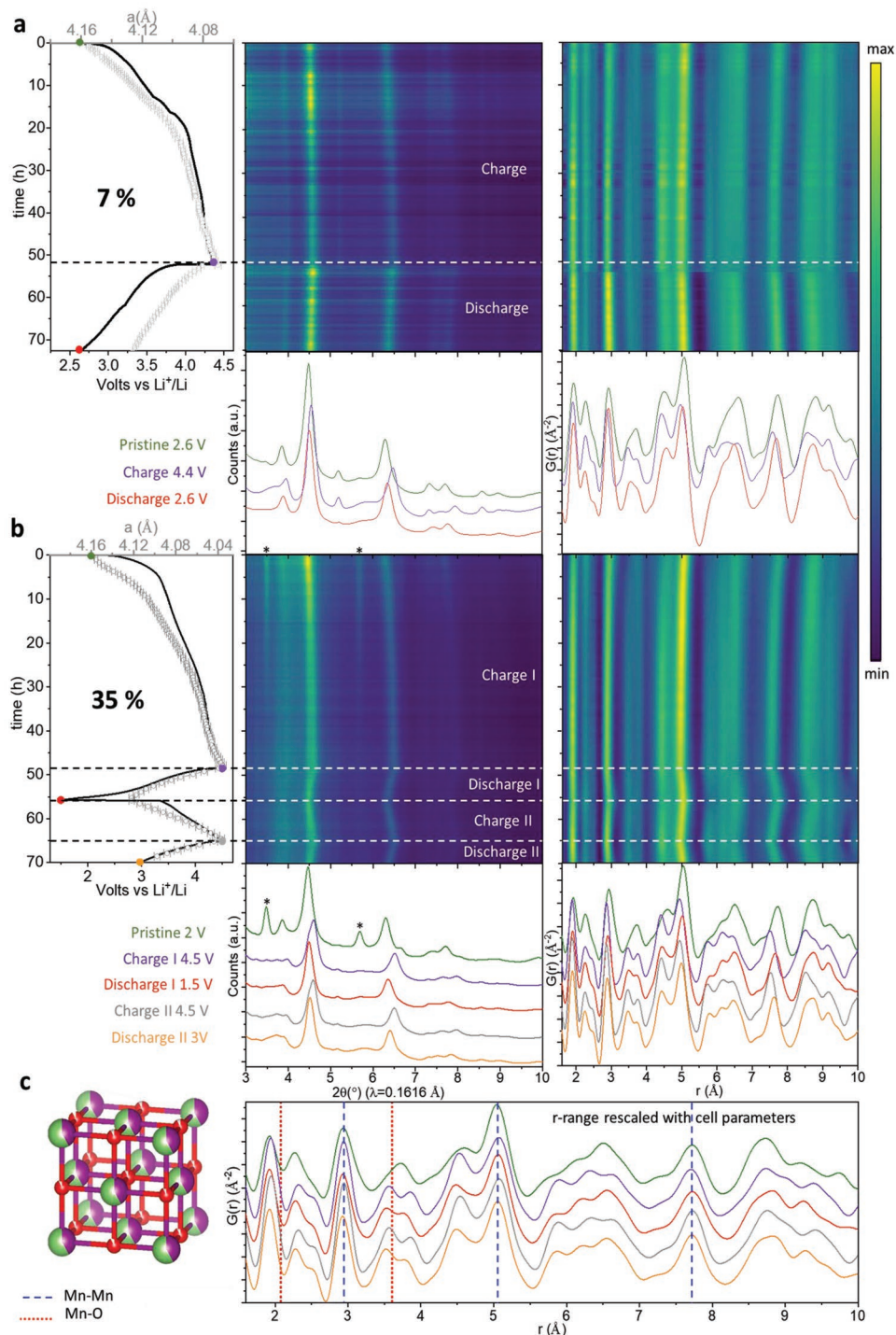


Figure 2. a) $0.07\text{Li}_2\text{O}:0.93\text{Li}_{2/3-x}\text{Mn}_{1/3}\text{O}_{5/6}$ and b) $0.35\text{Li}_2\text{O}:0.65\text{Li}_{2/3-x}\text{Mn}_{1/3}\text{O}_{5/6}$ evolution with cycling characterized by in situ X-ray total scattering. From left to right: electrochemical performance (solid line) overlaid with lattice parameters from a sequential Rietveld refinement (empty circles, where errors bars often lie underneath the symbols), reciprocal and real space (PDF) total scattering data. Bottom figures show the data at selected potential values marked by solid spheres in the electrochemical curve. c) $0.35\text{Li}_2\text{O}:0.65\text{Li}_{2/3-x}\text{Mn}_{1/3}\text{O}_{5/6}$ PDFs at selected potential values rescaled on the r -range by the lattice parameter ratio. Vertical lines indicate the expected distances in the average RS structure for the most strongly scattering atom pairs: Mn–Mn and Mn–O, see Figure S5 (Supporting Information) for all of the pair contributions to the PDF.

is unlikely to be responsible for the large capacities measured. Thus, Equation (1) is expected to be the dominant route for Li_2O decomposition.

The $0.55\text{Li}_2\text{O}:0.45\text{Li}_{2/3-x}\text{Mn}_{1/3}\text{O}_{5/6}$ nanocomposite with the best performance has been evaluated as an additive of LFP and LiCoO_2 cathodes cycled against Li metal in **Figure 3**.

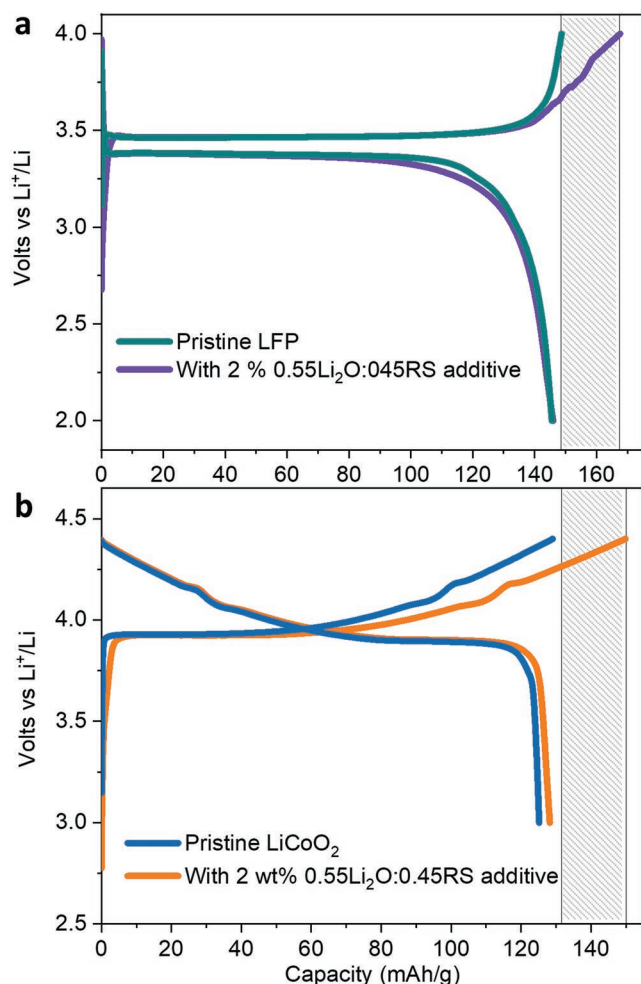


Figure 3. Improved first charge performance of a) LFP (green) with 2 wt% 0.55Li₂O:0.45Li_{2/3-x}Mn_{1/3}O_{5/6} sacrificial additive (purple), and b) LiCoO₂ (blue) with the same amount of additive (orange).

The electrochemical curves of the pristine cathodes and with 0.55Li₂O:0.45Li_{2/3-x}Mn_{1/3}O_{5/6} additive appear more different at 3.5–4 V due to a more predominant contribution to the charge capacity from the additive at the higher potential. The addition of 2 wt% of 0.55Li₂O:0.45Li_{2/3-x}Mn_{1/3}O_{5/6} resulted in a 13% increase of the first charge capacity, and matching discharge capacities to that of pristine LFP and LiCoO₂. Thus, while increasing the initial charge capacity, the sacrificial additive did not interfere with the electrochemical performance of the pristine cathode materials (see Figure S10 in the Supporting Information for cycling stability over 7–10 cycles). Note that the large initial charge capacity of 0.55Li₂O:0.45Li_{2/3-x}Mn_{1/3}O_{5/6} allows for the use of such small amount of additive of only 2 wt% (vs more routinely used 5–10 wt%^[11–13,19] to compensate for similar capacity losses). Moreover, ≈55 mol% of the sacrificial is consumed after the first charge and only <1 wt% remains in the cathode, and the smaller volumes of released gas versus sacrificial salts^[9] mitigate potentially detrimental effects related to gas evolution during battery cycling.

In summary, we propose a design principle for cathode prelithiation to compensate the first-cycle Li loss in Li-ion

batteries based on nanoscale mixtures of Li_{2/3-x}Mn_{1/3}O_{5/6} and Li₂O. The high prelithiation efficacy demonstrated exploits the irreversible electrochemical activation of Li₂O during the first charge. With such a cathode prelithiation additive, the first charge capacity of LFP and LiCoO₂ has been improved by 13%, while the subsequent discharge capacity matches that of the pristine cathode materials. Due to their low cost, ease of preparation, and potential compatibility with industrial battery fabrication, Li₂O:Li_{2/3-x}Mn_{1/3}O_{5/6} nanocomposites are highly promising additives for the prelithiation of cathode materials. The reported pretreatment could be applied to other Li-cathode materials, and seems extrapolable for the presodiation of Na-ion batteries based on initial tests on Na₂O:Na–Mn–O composites that showed an analogous irreversible electrochemical activation of Na₂O with improved first charge capacities.

Supporting Information

Supporting Information is available from the Wiley Online Library or from the author.

Acknowledgements

This work was supported by the ANR Grant No. ANR15-CE05-0006-01DAME. The authors acknowledge Jean Justine at the CRISMAT for technical assistance, Dr. Olivier Proux for support during beamtime at the FAME beamline (CRG-ESRF) and Diamond Light Source for time on beamline I15-1 under proposal EE20893.

Conflict of Interest

The authors declare no conflict of interest.

Keywords

cation-disordered rock salts, initial capacity losses, Li₄Mn₂O₅, lithium batteries, sacrificial

Received: August 27, 2019
Revised: November 11, 2019
Published online: January 12, 2020

- [1] Y. Matsumura, S. Wang, J. Mondori, *J. Electrochem. Soc.* **1995**, *142*, 2914.
- [2] C. K. Chan, R. Ruffo, S. Sae, Y. Cui, *J. Power Sources* **2009**, *189*, 1132.
- [3] N. Liu, L. Hu, M. T. Mcdowell, A. Jackson, Y. Cui, *ACS Nano* **2011**, *5*, 6487.
- [4] J. Hassoun, J. Kim, D. Lee, H. Jung, S. Lee, Y. Sun, B. Scrosati, *J. Power Sources* **2012**, *202*, 308.
- [5] C. R. Jarvis, M. J. Lain, M. V. Yakovleva, Y. Gao, *J. Power Sources* **2006**, *162*, 800.
- [6] Z. Wang, Y. Fu, Z. Zhang, S. Yuan, K. Amine, V. Battaglia, G. Liu, *J. Power Sources* **2014**, *260*, 57.
- [7] C. R. Jarvis, M. J. Lain, Y. Gao, M. Yakovleva, *J. Power Sources* **2005**, *146*, 331.
- [8] J. Zhao, Z. Lu, N. Liu, H. Lee, M. T. Mcdowell, Y. Cui, *Nat. Commun.* **2014**, *5*, 5088.

- [9] D. Shanmukaraj, S. Grugeon, S. Laruelle, G. Douglade, J. M. Tarascon, M. Armand, *Electrochem. Commun.* **2010**, *12*, 1344.
- [10] X. Bian, Q. Pang, Y. Wei, D. Zhang, Y. Gao, G. Chen, *Chem. - Eur. J.* **2018**, *24*, 13815.
- [11] K. West, G. Vitins, R. Koksang, *Electrochim. Acta* **2000**, *45*, 3141.
- [12] M. Gyu, J. Cho, *J. Mater. Chem.* **2008**, *3*, 5880.
- [13] M. Noh, J. Cho, *J. Electrochem. Soc.* **2012**, *159*, 1329.
- [14] G. Vitins, E. A. Raekelboom, M. T. Weller, J. R. Owen, *J. Power Sources* **2003**, *119–121*, 938.
- [15] J. Cabana, L. Monconduit, D. Larcher, M. R. Palacín, *Adv. Energy Mater.* **2010**, *22*, E170.
- [16] K. Cao, T. Jin, L. Jiao, *Mater. Chem. Front.* **2017**, *1*, 2213.
- [17] Y. Sun, H.-W. Lee, Z.-W. Seh, N. Liu, J. Sun, Y. Li, Y. Cui, *Nat. Energy* **2016**, *1*, 15008.
- [18] Y. Sun, H.-W. Lee, Z. W. Seh, G. Y. Zheng, J. Sun, Y. B. Li, Y. Cui, *Adv. Energy Mater.* **2016**, *6*, 1600154.
- [19] Y. Sun, H. Lee, G. Zheng, Z. W. Sen, J. Sun, Y. Li, Y. Cui, *Nano Lett.* **2016**, *16*, 1497.
- [20] K. Park, B.-C. Yu, J. B. Goodenough, *Adv. Energy Mater.* **2016**, *6*, 1502534.
- [21] M. Freire, N. V. Kosova, C. Jordy, D. Chateigner, O. I. Lebedev, A. Maignan, V. Pralong, *Nat. Mater.* **2015**, *15*, 173.
- [22] N. Yabuuchi, M. Takeuchi, S. Komaba, S. Ichikawa, T. Ozaki, T. Inamasu, *Chem. Commun.* **2016**, *52*, 2051.
- [23] N. Takeda, S. Hoshino, L. Xie, S. Chen, I. Ikeuchi, R. Natsui, K. Nakura, N. Yabuuchi, *J. Power Sources* **2017**, *367*, 122.
- [24] R. A. House, L. Jin, U. Maitra, K. Tsuruta, J. W. Somerville, D. P. Fo, F. Massel, L. Duda, M. R. Roberts, P. G. Bruce, *Energy Environ. Sci.* **2018**, *11*, 926.
- [25] R. Wang, X. Li, L. Liu, J. Lee, D. H. Seo, S. H. Bo, A. Urban, G. Ceder, *Electrochem. Commun.* **2015**, *60*, 70.
- [26] J. Lee, D. A. Kitchaev, D. Kwon, C. Lee, J. K. Papp, Y. Liu, Z. Lun, *Nature* **2018**, *556*, 185.
- [27] T. Kobayashi, W. Zhao, H. B. Rajendra, K. Yamanaka, *Small* **2019**, *15*, 1902462.
- [28] M. Freire, M. Diaz-Lopez, P. Bordet, C. V. Colin, O. I. Lebedev, N. V. Kosova, C. Jordy, D. Chateigner, A. L. Chuvilin, A. Maignan, V. Pralong, *J. Mater. Chem. A* **2018**, *6*, 5156.
- [29] M. Diaz-Lopez, Y. Joly, M. Freire, C. Colin, O. Proux, V. Pralong, P. Bordet, *J. Phys. Chem. C* **2018**, *122*, 29586.
- [30] P. Poizot, S. Laruelle, S. Grugeon, L. Dupont, J. Tarascon, *Nature* **2000**, *407*, 496.
- [31] S. A. Freunberger, Y. Chen, Z. Peng, J. M. Gri, L. J. Hardwick, P. Nov, P. G. Bruce, *J. Am. Chem. Soc.* **2011**, *133*, 8040.